Role of contacts in long-range protein conductance

Bintian Zhang[a], Weisi Song[a], Pei Pang[a], Huafang Lai[a], Qiang Chen[a,b], Peiming Zhang[a], and Stuart Lindsay[a,c,d,1]

[a]Biodesign Institute, Arizona State University, Tempe, AZ 85287; [b]School of Life Sciences, Arizona State University, Tempe, AZ 85287; [c]Department of Physics, Arizona State University, Tempe, AZ 85287; and [d]School of Molecular Sciences, Arizona State University, Tempe, AZ 85287

Edited by Harry B. Gray, California Institute of Technology, Pasadena, CA, and approved February 4, 2019 (received for review November 16, 2018)

Proteins are widely regarded as insulators, despite reports of electrical conductivity. Here we use measurements of single proteins between electrodes, in their natural aqueous environment to show that the factor controlling measured conductance is the nature of the electrical contact to the protein, and that specific ligands make highly selective electrical contacts. Using six proteins that lack known electrochemical activity, and measuring in a potential region where no ion current flows, we find characteristic peaks in the distributions of measured single-molecule conductances. These peaks depend on the contact chemistry, and hence, on the current path through the protein. In consequence, the measured conductance distribution is sensitive to changes in this path caused by ligand binding, as shown with streptavidin–biotin complexes. Measured conductances are on the order of nanosiemens over distances of many nanometers, orders of magnitude more than could be accounted for by electron tunneling. The current is dominated by contact resistance, so the conductance for a given path is independent of the distance between electrodes, as long as the contact points on the protein can span the gap between electrodes. While there is no currently known biological role for high electronic conductance, its dependence on specific contacts has important technological implications, because no current is observed at all without at least one strongly bonded contact, so direct electrical detection is a highly selective and label-free single-molecule detection method. We demonstrate single-molecule, highly specific, label- and background free-electronic detection of IgG antibodies to HIV and Ebola viruses.

protein electronics | molecular electronics | single-molecule conductance | protein detection | label-free detection

Proteins lack electronic conduction bands because the interactions that facilitate hopping are weak compared with the vibronic coupling (1) and also because they are not highly ordered [but see Vattay et al. (2)]. Nonetheless, long-range electron transport can occur when energetic carriers are injected at potentials that exceed the redox potentials of amino acid residues in the protein. The use of chromophores to allow optical injection of carriers at well-defined energies has enabled a detailed elaboration of charge-transfer pathways in many cases (3, 4). When proteins are contacted by metal electrodes, the situation is more complicated (5, 6). Single-protein conductances of nanosiemens (nS) over nanometer (nm) distances have been reported (7), with essentially the same conductance measured across a 2-nm protein (8) as across a 5.4-nm protein (9); temperature-independent transport has been observed (10) and siemens per meter conductivities over micrometers have been reported in bacterial pili (11, 12). Carrier injection via a contact is extremely sensitive to surface charge at the interface, with different preparations of oxide barrier at a semiconductor interface being the determining factor in whether electron transport in bacteriorhodopsin is temperature dependent or not (13). Accordingly, a reproducible method for forming electrical contacts is highly desirable. In addition, these prior studies are subject to uncertainties about the number of molecules contacted, the size of the gap, the nature of the contacts, and possible ionic contributions to current. Here, we report single-molecule measurements made using ligand-functionalized electrodes in solution under potential control, with electrode potentials set such that no significant ionic current flows. We find that the binding of a ligand specific to a particular protein forms an excellent electrical contact: The conditions for specific binding are also the conditions for charge injection. The specificity of ligands on electrode surfaces also serves to indicate that proteins are still functionally selective on these electrode surfaces.

Single-Molecule Conductance Measurements

Reproducible two-point measurements of the conductance of molecules require reproducible contacts (14), so the reproducible observation of large (nS-scale) conductance fluctuations in single integrin molecules (bound to just one of two electrodes by their cognate ligands) was a surprising finding (15). This prior work did not probe the low bias region (where fluctuations were absent) owing to leakage currents that obscured any dc current through the protein. In the present study, we used a scanning tunneling microscope (STM) to make single-molecule measurements in solution (Fig. 1*A*), systematically exploring the role of contacts, both specific and nonspecific (Fig. 1*B*). With suitably insulated STM probes (16) and potential control of the electrodes (*Methods* and *SI Appendix*, Fig. S1), the background leakage current was reduced to less than 1 pA over the entire bias range. With adequate stabilization, the STM gap remained constant over periods of a minute (*Methods* and *SI Appendix*, Fig. S2) so we were able to disable the gap control servo, retract the tip, and record current–voltage (IV) curves. Up to 60 such curves (sweeping both up and down) were recorded before reengaging the servo and repeating

Significance

The measured electronic properties of proteins are known to depend critically on contacts, although little is known at the single-molecule level. Here, we have measured the conductance of single-protein molecules in their natural aqueous environment, but in conditions where no ion current flows, finding large conductances (nanosiemens) over long paths (many nanometers) when the protein is tethered by chemical contacts formed by binding-specific ligands. This provides a method for forming reliable contacts to proteins, and for the specific detection of single molecules. Thus, single antibodies, such as anti-Ebola IgG, can be detected electrically when they bind a peptide epitope tethered to electrodes, with no background signal from molecules that do not bind specifically.

Author contributions: B.Z., P.Z., and S.L. designed research; B.Z. and W.S. performed research; W.S., P.P., H.L., and Q.C. contributed new reagents/analytic tools; W.S. and S.L. analyzed data; and S.L. wrote the paper.

Conflict of interest statement: P.Z. and S.L. are inventors of a technology described in a provisional patent application "Device, System and Method for Direct Electrical Measurement of Enzyme Activity."

This article is a PNAS Direct Submission.

[1]To whom correspondence should be addressed. Email: stuart.lindsay@asu.edu.

This article contains supporting information online at www.pnas.org/lookup/suppl/doi:10.1073/pnas.1819674116/-/DCSupplemental.

Published online March 7, 2019.

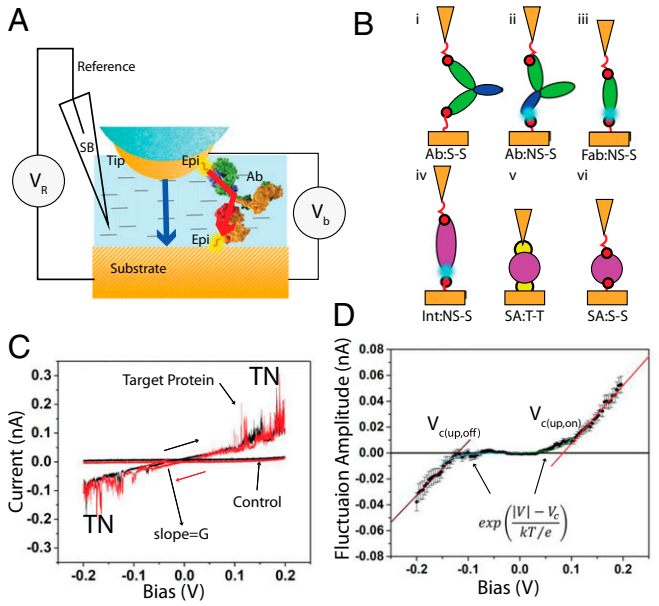

Fig. 1. Measuring the conductance of single-protein molecules in solution. (*A*) STM with Pd probe and substrate functionalized with epitopes (Epi) that capture a cognate antibody (Ab). A bias V_b is applied with one of the electrodes held at V_R relative to a reference electrode (*SI Appendix*, Fig. S1). Tip insulation (blue) reduces leakage currents to <1 pA. Transport is through-molecule (red arrow) not through-space (blue arrow). (*B*) Bonding schemes, red = specific (S), turquoise = nonspecific (NS), yellow = thiol to metal (T): (*i*) antibody, S-S; (*ii*) antibody NS-S; (*iii*) Fab fragment, (NS-S): (*iv*) integrin (NS-S); (*v*) thiolated-streptavidin, (T-T); (*vi*) apo-streptavidin binding biotin (S-S). (*C*) IV curve for anti-DNP binding DNP in a 4.5-nm gap (see *SI Appendix*, Fig. S3 for other proteins). The IV response (black) is linear and reproduced on the down-sweep (red) (slope = conductance, *G*). Homologous control proteins gave no signals. TN appears above ~ ±0.1 V, with the turn-on bias, V_C, obtained from fits (colored lines in *D*) as described in *SI Appendix*, Fig. S5. (*D*) Averaged TN amplitudes for 1,205 up-sweep curves (anti-DNP at a 3.5-nm gap, error bars are ±1 SE) showing the turn-on at ±0.1 V. Fitting parameters for all gap values are shown in *SI Appendix*, Figs. S5 and S6.

the process on another area of the substrate. To make two specific contacts, we have used bivalent antibodies (an IgE and two IgGs), each of which presents two binding sites, as well as streptavidin which binds up to four biotin molecules, so that epitope- or biotin-functionalized electrodes could be bridged by specific bonds. In the cases where bare metal electrodes were used, contacts were made to surface thiols on streptavidin modified with an average of 2.5 surface thiols per molecule. In addition, we repeated measurements using integrin, which can form a specific bond with only one of the two peptide-functionalized electrodes. Proteins and ligands are listed in Table 1 and the various bonding arrangements are shown schematically in Fig. 1*B*.

Measured Conductances Depend on Contacts

Currents were only observed when the protein was bound specifically to at least one of the two electrodes and a representative IV curve for antidinitrophenol (anti-DNP) binding DNP-coated electrodes is shown in Fig. 1*C* (examples are given in *SI Appendix*, Fig. S3 for the other proteins). The trace shown here is for a tip retraction of 2 nm for an overall gap of ~4.5 nm, given that, at the 20-picosiemen (pS) set-point (4 pA at 0.2 V), the gap is ~2.5 nm (17). Typically, no current was recorded for several seconds after retraction, after which the current jumped to a large (and variable) value in the presence of bound protein. Examples of current vs. time recordings at a constant 50-mV bias are shown in *SI Appendix*, Fig. S4 *A* and *B*. Although the current fluctuates over minute timescales, it is usually stable over a few seconds, so that 80% of the recorded curves on the sweep up (black trace) are reproduced on the sweep down (red trace). Controls (buffer alone or noncognate proteins in solution) gave no signals. The rapidly fluctuating (millisecond-timescale) telegraph noise (TN) reported (15) for integrin is also observed here for anti-DNP (Fig. 1 *C* and *D*), and all of the other proteins studied (*SI Appendix*, Fig. S3) above 0.1 V. It is a ubiquitous signal of protein capture, showing the same two-level switching in all cases. We originally observed these fluctuations for a protein captured in a fixed-junction chip (15) and although the present work uses an STM, we have replicated measurements of TN for one of the proteins studied here (anti-DNP) in a chip as well as in the STM to show that these are not some artifact of the measurement method. Examples of this TN are given in *SI Appendix*, Fig. S7. The voltage threshold for TN does not depend on gap until the contact is almost broken (see Fig. 3*E* and *SI Appendix*, Figs. S5 and S6), implying that it is associated with fluctuations of the contacts driven by a potential drop that occurs mostly at the contacts, as previously proposed (15) and discussed in more detail below.

With the exception of the TN, the response is linear, so that each IV trace can be characterized by a single conductance value, G. Measured distributions of G are shown in Fig. 2, and they follow the log-normal distribution usually observed in single-molecule measurements (18). The distributions are similar to distributions of current values obtained by recording current vs. time at a fixed gap and bias (*SI Appendix*, Fig. S4 *C* and *D*) so we ascribe the distribution to different kinds of contact between the electrodes and the molecule. The distributions for integrin (gap = 4.5 nm) and thio-streptavidin (gap = 2.5 nm) have a single peak at about 0.3 nS (Fig. 2*A*). Bare metal electrodes were used to capture the thiolated streptavidin, where the thiol-mediated (T-T in Fig. 1 *B*, *v*) contacts displace the contamination on the electrode surfaces (19), forming direct metal–molecule contacts. The integrin was captured by the cyclic RGD peptide [cyclo (Arg-Gly-Asp-D-Phe-Cys)] at only one of the two electrodes, and no signals were observed unless both electrodes were functionalized. Functionalization with peptides allows for nonspecific contacts with hydrophilic sites on the protein at the electrode that is not specifically coupled (NS-S, Fig. 1 *B*, *iv*). The three antibodies (Fig. 2) yielded two conductance peaks (~0.3 and ~2 nS), suggesting two binding modes: NS-S (Fig. 1 *B*, *ii*) as for the integrin, and the desired S-S (Fig. 1 *B*, *i*) when both antigen-binding sites bind specifically. We tested this interpretation by replacing the peptides on one electrode with mercaptoethanol, making it hydrophilic and capable of forming an NS-S bridge (Fig. 1 *B*, *ii*). Only a single peak was observed (Fig. 2*B*). As a further test, we prepared a Fab fragment from the anti-Ebola IgG with only a monovalent binding head. The fragment was too small to bridge the 4.5-nm gap, so the data shown in Fig. 2*B* were recorded in a 2.5-nm gap. There is only a single peak in the conductance distribution, reflecting the single NS-S contact (Fig. 1 *B*, *iii*). Thus, the higher-conductance peak must correspond to conduction via the two antigen binding sites. In order for this effect to be seen, the dataset must be dominated by single-molecule contacts. It is striking that the conductance of a single Fab fragment across a 2.5-nm gap is much smaller than the conductance of an antibody across a 4.5-nm gap (Fig. 2*B*). This suggests that the intrinsic internal conductances of the proteins are much higher than the measured (contact-limited) values. This finding accounts for the previous reports of similar conductances measured for proteins of very different sizes (5, 6).

Table 1. Proteins and ligands used in this study; cysteine or thiol used for electrode attachment is shown in red

Target	MW, kDa	Height, nm	Probe on electrodes	K_D	Control	Peak conductance (nS)	Binding mode (Fig. 1*B*)
IgE anti-DNP	190	~5*	HSCH_2CH_2-dinitrophenol	65 nM	IgE isotype	0.27 ± 0.03, 1.96 ± 0.47	NS-S S-S
IgG anti-HIV	150	~7†	CALDRWEKIRLR	240 nM	IgG isotype	0.33 ± 0.03, 2.18 ± 0.36	NS-S S-S
IgG anti-Ebola	175	~7†	CHNTPVYKLDISEATQV	1400 nM	IgG isotype	0.26 ± 0.007, 2.09 ± 0.09	NS-S S-S
Fab anti-Ebola	50	~4‡	CHNTPVYKLDISEATQV	NA	IgG isotype	0.30 ± 0.008	NS-S
$\alpha_V\beta_3$ integrin	190	~10§	Cyclic RGDfC	~10 nM	$\alpha_4\beta_1$ integrin	0.38 ± 0.009	NS-S
Biotin	NA	NA	Thiolated-streptavidin	~10 fM	NA	0.35 ± 0.008	T-T
Streptavidin	55	~3.5¶	HSCH_2CH_2-biotin	~10 fM	NA	0.26 ± 0.01, 1.48 ± 0.07, 6.80 ± 0.6	S-S

Linear dimensions are from the RSCB PDB, either across a minor diameter or, for the antibodies, binding head to binding head.
*IgE structure 4GRG.
†IgG, structure 4NHH.
‡Fab fragment structure 1YUH.
§Integrin structure 1L5G.
¶Streptavidin structure 1VWA.

Conductances Do Not Depend on Gap Size

The existence of an internal [through-molecule (20)] high-conductance path is illustrated by a series of measurements taken at different gap sizes, using the technique described above, but increasing the amount of the initial tip retraction (Fig. 3). Strikingly, the peak conductance values do not change with the gap size (Fig. 3*E* and *SI Appendix*, Table S2) although the frequency with which data are accumulated falls (*SI Appendix*, Table S1). This effect reflects the area of the probe available for contacts at a given height, as illustrated in Fig. 3 (*Left*). Very few sites are available when the gap is comparable to the protein height (listed for similar structures found in the protein database in Table 1). Gap-independent conductance has been reported before for azurin [see the SI of Ruiz et al. (21)] and a rod-like molecule trapped between a probe and a substrate (20). As pointed out above, the contact point changes over the (~minute) course of a measurement, a reflection of the angstrom-scale change in the position of the STM probe. It is these various contact geometries that generate the overall shape of the conductance distributions (*SI Appendix*, Fig. S4). Since the distributions retain the same peak positions and shapes at the different gap sizes, the data show no indications of proteins being "squeezed" at the smaller gap sizes.

Fig. 3*E* also plots the voltage thresholds for the turn-on of TN as a function of gap size. They also do not change significantly with the gap size. Thus, TN fluctuations must be driven by the local field at the metal–molecule interface, with relatively little potential dropped across the interior of the protein. This is also consistent with our finding that the lifetime of the TN is exponentially related to the peak current value, an observation that

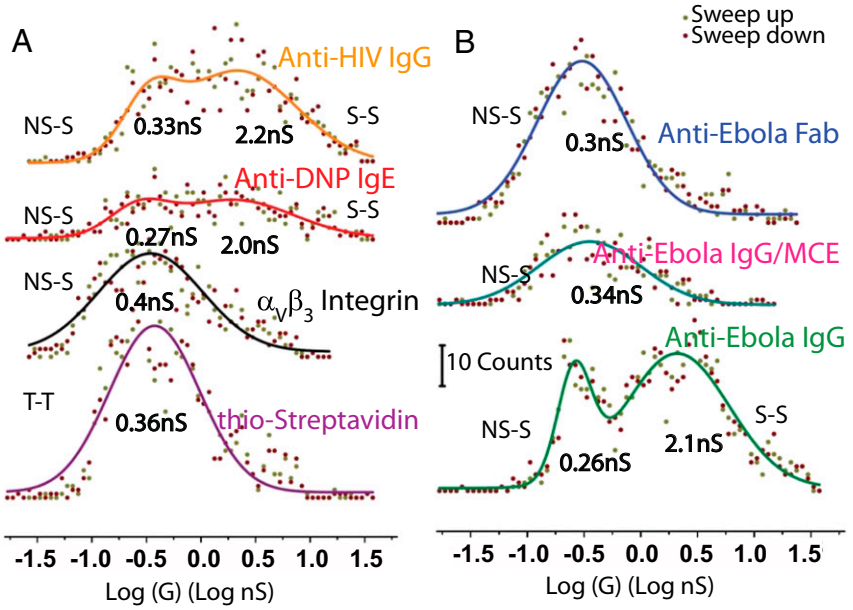

Fig. 2. Protein conductance distributions are controlled by contacts. (*A*) Conductance distributions for molecules with one bonding path (T-T, NS-S) have one peak. Antibodies which can bind via NS-S or S-S paths have two. (*B*) Distribution for anti-Ebola IgG, showing the two peaks and (traces above) how the higher conductance (S-S) peak is suppressed when one electrode is coated with a nonspecifically binding reagent (mercaptoethanol) or when both electrodes are coated with the epitope but a monovalent Fab fragment is used. Data were acquired with V_R = 0 V against a 10 mM reference (*SI Appendix*, Figs. S1 and S8) with a gap of 2.5 nm for the small proteins (streptavidin, Fab) and 4.5 nm for the larger proteins.

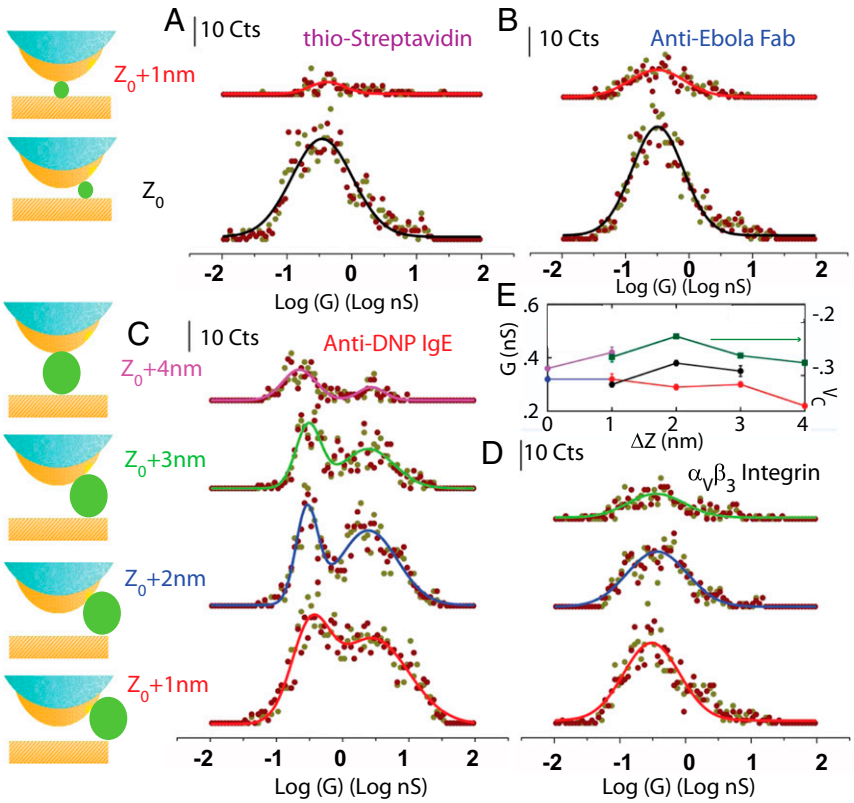

Fig. 3. Conductances do not change with gap so path is through-molecule and intrinsic conductance is higher than contact-limited conductance. Conductance distributions taken at a series of different gaps for (*A*) streptavidin, (*B*) anti-Ebola Fab, (*C*) anti-DNP, and (*D*) integrin (*SI Appendix*, Table S2 lists fitting parameters). The frequency of successful contacts is reduced as the gap is increased (*SI Appendix*, Table S1), likely reflecting the gap geometry as illustrated on the left. (*E*) Fitted values of peak conductance (dots: purple streptavidin; blue: Ebola Fab; red: anti-DNP; black: integrin); and threshold voltage, V_c, for the onset of conductance fluctuations in anti-DNP (green squares, right axis) do not change with gap. See *SI Appendix*, Figs. S5 and S6 for distance dependence of other parameters.

can be accounted for by a single "weak-link" tunneling junction in the circuit that dominates the conductance (15).

Conductance Is Sensitive to Changes of Protein Structure

Since the conductance path follows the protein geometry, either internally or along a surface contour, changes in protein geometry, and thus in the conduction path, could affect which contact points control the conductance. This would enable direct electrical sensing of structural changes of the protein. We demonstrate this effect in Fig. 4 *A* and *B*. Fig. 4*A* shows the conductance distribution (replicating the data in Fig. 2*A*) for a thiolated-streptavidin sample that was subsequently incubated with biotin (1 mM for 1 h), a process that alters the structure of the streptavidin tetramer substantially (22). Biotin complexation changes the conductance distribution significantly (Fig. 4*B*). A streptavidin molecule has four biotin binding sites (23), so that the unthiolated apo-protein can be cross-linked by two biotins (S-S in Fig. 1 *B*, *vi*). We synthesized a thiolated biotin (*Methods*) and functionalized both the probe and substrate with it (Fig. 4*C*), subsequently flowing apo-streptavidin into the sample cell. The consequent G distribution had three peaks, with the highest at nearly 7 nS. Thus, the measured conductance is sensitive to both local changes in protein structure and the chemical nature of the contact, showing how contacts are affected by structural changes of the protein. We also attached thiolated streptavidin to the substrate and probed it with a biotinylated probe with similar results (Fig. 4*D*) demonstrating that a single biotin-mediated contact is sufficient to generate the high-conductance state at ∼7 nS.

Possible Mechanisms

Electron tunneling decays far too rapidly to account for long-range transport. A tunneling conductance can be estimated from $G \sim G_0 \exp(-\beta x)$ where G_0 is 77 μS and $\beta \sim 1$ Å^{-1} (24). For a small protein with $x \sim 4$ nm, this yields $G < 10^{-21}$ S, 12 orders of magnitude smaller than observed. To account for the observation of nS conductance over 10-nm distances would require a $\beta <$ 0.1 Å^{-1}. In the well-studied case of DNA, thermally activated hopping (25) leads to nearly distance-independent transport when the distance between the readily ionized guanines exceeds three nucleotides (26). Similar transport (via readily oxidized amino acids) has been observed in peptides (4). In these cases, transport was limited by charge injection, and the ∼1.5-eV barrier to charge injection was overcome using a chromophore excited with 630-nm (∼2-eV) light. If a similar transport mechanism operates in the case of charge injection from electrodes, the barrier would be determined by the energy gap between the Fermi energy of Pd (work function 5.2 eV) and the absolute redox potential of the readily oxidized residues tyrosine and tryptophan. These potentials are ∼+1 to + 1.2 V vs. the normal hydrogen electrode (NHE) (27, 28) so using 4.4 eV for the work function of the NHE (29) gives absolute potentials around 5.4–5.6 eV below the vacuum or a barrier of +0.2–0.4 eV with respect to the Fermi energy of Pd. Thus, a barrier of this magnitude must be overcome by the bond polarization associated with the binding of the protein to the electrode. This is well within the range of work-function changes observed for small molecules attached to a noble-metal surface by a thiol linkage (30). We obtain significant currents in three situations: (*i*) when contacts

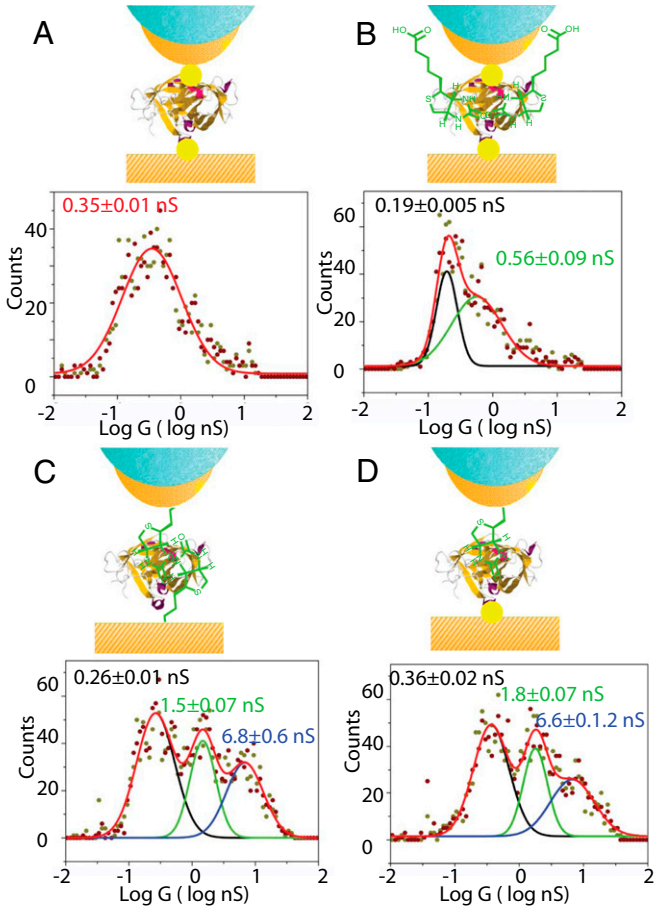

Fig. 4. Conductance changes on ligand binding and also with the chemistry of the contact. Distribution for thiolated-streptavidin (*A*) and for the same sample after incubation with biotin (*B*). The single conductance peak changes to two peaks with significantly different values. Streptavidin captured by biotin probes on the electrodes (*C*) has an additional feature of much higher conductance. These features are retained with one thiol bond and one biotin bond (*D*). Biotin size is exaggerated for clarity.

to both electrodes are via direct, thiol-mediated bonding; (*ii*) when one bond is formed by specific binding to an epitope or ligand and another is formed by nonspecific interactions between hydrophilic molecules attached to the electrode and the hydrophilic exterior of a protein and (*iii*) the largest currents are observed when the protein is bound by recognition ligands at both electrodes (the ligand being linked via thiols to the electrodes in all cases). Weak, nonspecific bonds do not result in significant current flow: At least one attachment must be via a covalent or ligand-mediated linkage. Thus, the barrier to charge injection is overcome by the binding of at least one specific ligand if the protein itself is not covalently modified to bind directly to the electrode.

Small changes in interfacial charge at a contact have been shown to affect transport strongly (13) and this is a variable we can change using potential control, albeit only over a small range if Faradaic currents are to be avoided. *SI Appendix*, Fig. S8 shows the small changes in the conductance distributions caused by a small positive surface charge (+50 mV vs. the 10-mM Ag/AgCl reference). Presumably, these small changes are dominated by a much larger field owing to bond polarization at the interface. In addition to the redox potentials of amino acid residues, the 3D folding of the protein must play an important role. This is because small peptides that are stretched in a break junction do not conduct (24), whereas similar small peptides, folded on an electrode surface, do conduct (31). This could be a consequence of some special geometry (32) or arrangement of hydrogen bonds (33).

We turn finally to the fluctuations that set in above ±100-mV applied bias. The small dependence of this threshold voltage on gap size (Fig. 3*E* and *SI Appendix*, Fig. S6) is consistent with the hypothesis that the internal conductance of the proteins is much higher than the conductance at the contacts, implying that these signals arise from voltage-driven fluctuations of the contacts themselves. We proposed such a mechanism in our earlier study of integrin (15), where we showed that the lifetime of the "on" states, τ, was related to the peak current, i_p, of the telegraph noise peaks via $\tau \propto \ln(i_p)$, a relationship that can be explained by means of a single barrier determining both current and bonding strength. *SI Appendix*, Fig. S5 shows that, once turned on, the current grows linearly with voltage, indicating that an Ohmic conductance channel opens. The turn-on process is described by an exponential of the form $\exp\left(\frac{|V|-V_c}{kT/e}\right)$, where V_c is an activation voltage. Fits yield $V_c \sim 0.25$ V, a value characteristic of hydrogen bond strengths in water (34) suggesting that a hydrogen bond may be the weak link in the circuit.

It is interesting to note that this 0.25-V barrier is similar to the charge-injection barrier deduced from the redox potentials of the amino acids, as discussed above. If the charge-injection rate was limited by thermally activated hopping over a 0.22–0.47-V barrier, and it is this rate that determines the conductance, then we would expect to observe a conductance of $\approx G_0 \exp\left(-\frac{V}{ckT_B}\right)$, where $0.22 < V < 0.47$ V, yielding from 12 nS to 0.5 pS, a range which encompasses the values reported here.

Role of Specific Binding in Electronic Conductance

We conclude that specific ligand–receptor interactions form good electrical connections to proteins. This is illustrated by the data shown in Fig. 4 *B*–*D*. Connections made via covalent (thiol) modification of surface lysines directly bonded to the metal electrodes yield a lower maximum conductance (0.56 nS) than the noncovalent streptavidin–biotin coupling linked to the electrodes via a thiol-terminated ethane linkage (6.8 nS). This conductance is barely altered when only one biotinylated linker is used (Fig. 4*D*). Thus, a weaker coupling to the hydrophobic interior of a protein is more effective than a stronger coupling to the hydrophilic exterior, even if only one such coupling is made. If, once injected, electrons move readily in the interior of the protein, then a second (nonspecific) contact will act only as a barrier at the hydrophilic surface of the protein. Such a mechanism would account for the high conductance of integrin when bound by a ligand at only one site, and also for the complete lack of conductance when both contacts are noncovalent and nonspecific.

Future Applications

The fact that specific ligands make excellent electrical connections clearly has technological implications. The requirement of at least one specific bond for conduction means that there is no background signal at all in the presence of proteins that do not bind the electrode-tethered capture probes or react directly with electrodes, in contrast to fluorescent tags for which background signal is always present. Thus, direct, label-free, sensitive, and very selective (background-free) single-molecule detection may be possible. Another application may lie in dynamic recording of conductance changes. Electrostatic sensing has been used to record enzyme motions on sub-ms timescales (35), and the sensitivity of conductance to structural changes in a protein raises the possibility of direct electrical sensing of these motions, possibly enabling real-time recording of enzyme motions.

Methods

Functionalizing Substrates and STM Probes. Palladium substrates for STM measurement were prepared by evaporating a 200-nm palladium film onto a silicon wafer using an electron-beam evaporator (Lesker PVD 75), with a 10-nm titanium adhesion layer. The substrates were treated with a hydrogen flame immediately before functionalizing and then immersed in solutions of thiolated DNP, biotin, streptavidin, or peptides containing a cysteine residue, overnight. Substrate functionalization with small ligands was characterized by Fourier transform infrared spectroscopy (*SI Appendix*, Fig. S9) and ellipsometry. Coverage of the substrate was monitored by STM and atomic force microscopy imaging (*SI Appendix*, Figs. S10 and S11).

STM probes were etched from a 0.25-mm Pd wire (California Fine Wires) by an ac electrochemical method. To avoid current leakage, probes were insulated with high-density polyethylene following the method described earlier for gold probes (16). Each probe was tested by STM in 1 mM PB buffer at −0.5-V bias to ensure the leakage current was <1 pA. For functionalization, the probe was immersed in ligand solutions for 4 h or overnight. After that, it was taken out, rinsed with water, gently blown dry with nitrogen gas, and used immediately. Further details of the STM measurements are given in *SI Appendix*.

Sources of Materials. RGD peptide was purchased from Peptides International. Peptide ligands for the anti-HIV antibody and the anti-Ebola antibody were synthesized by CPC Scientific with a purity >95%. DNP and biotin disulfides were synthesized in our laboratory (*SI Appendix*, Figs. S12 and S13) and reduced for 2 h before use by an immobilized (Tris[2-carboxyethyl] phosphine hydrochloride) disulfide reducing gel from Thermo Scientific (catalog number 77712) following the manufacturer's instructions. Preparation of the solutions used in this work is described in *SI Appendix*. Anti-DNP antibody (mouse monoclonal IgE antibody), wild-type streptavidin, and all other chemicals were purchased from Sigma Aldrich. Anti-HIV antibody (Anti-HIV1 p17 antibody [32/1.24.89]) and all of the isotype controls were obtained from Abcam. Anti-Ebola antibody was cultured from plants as described in *SI Appendix*. Binding affinities of all of the three antibodies were measured by surface plasmon resonance. Thiolated streptavidin with an average of 2.5 thiols per tetramer was from ProteinMods. Ag/AgCl reference electrodes salt-bridged by 3 M KCl or 10 mM KCl were prepared as described previously (15). Full details of the cyclic voltammetry are provided in *SI Appendix*. The anti-Ebola antibody and the corresponding monomeric Fab fragment were prepared and purified as described in *SI Appendix*.

ACKNOWLEDGMENTS. Dr. Quan Qing made many useful suggestions during the course of this work, including the design of reference electrodes that are stable in protein solutions. Ben Miller synthesized all custom reagents. Stephen Johnson suggested the use of a Fab fragment as a control. Ismael Diez-Perez, David Cahen, Tom Moore, and Jan Mol made useful comments on the draft manuscript, and Gabor Vattay and David Beratan contributed to the discussion of the theoretical background. This work was funded in part by the National Human Genome Research Institute (Grant R01 HG009180), Recognition AnalytiX LLC, and the Edward and Nadine Carson Endowment.

1. Nitzan A (2006) *Chemical Dynamics in Condensed Phases* (Oxford Univ Press, Oxford).
2. Vattay G, Kauffman S, Niiranen S (2014) Quantum biology on the edge of quantum chaos. *PLoS One* 9:e89017.
3. Giese B, et al. (2005) Multistep electron transfer in oligopeptides: Direct observation of radical cation intermediates. *Angew Chem Int Ed Engl* 44:4073–4075.
4. Aubert C, Vos MH, Mathis P, Eker AP, Brettel K (2000) Intraprotein radical transfer during photoactivation of DNA photolyase. *Nature* 405:586–590.
5. Bostick CD, et al. (2018) Protein bioelectronics: A review of what we do and do not know. *Rep Prog Phys* 81:026601.
6. Amdursky N, et al. (2014) Electronic transport via proteins. *Adv Mater* 26:7142–7161.
7. Artés JM, Díez-Pérez I, Gorostiza P (2012) Transistor-like behavior of single metalloprotein junctions. *Nano Lett* 12:2679–2684.
8. Yoo S-Y, Lee T, Chung Y-H, Min J, Choi J-W (2011) Fabrication of biofilm in nanoscale consisting of cytochrome f/2-MAA bilayer on Au surface for bioelectronic devices by self-assembly technique. *J Nanosci Nanotechnol* 11:7069–7072.
9. Korpany KV, et al. (2012) Conductance switching in the photoswitchable protein Dronpa. *J Am Chem Soc* 134:16119–16122.
10. Sepunaru L, Pecht I, Sheves M, Cahen D (2011) Solid-state electron transport across azurin: From a temperature-independent to a temperature-activated mechanism. *J Am Chem Soc* 133:2421–2423.
11. Adhikari RY, Malvankar NS, Tuominen MT, Lovley DR (2016) Conductivity of individual Geobacter pili. *RSC Adv* 6:8354–8357.
12. Malvankar NS, et al. (2011) Tunable metallic-like conductivity in microbial nanowire networks. *Nat Nanotechnol* 6:573–579.
13. Garg K, et al. (2018) Interface electrostatics dictates the electron transport via bioelectronic junctions. *ACS Appl Mater Interfaces* 10:41599–41607.
14. Cui XD, et al. (2001) Reproducible measurement of single-molecule conductivity. *Science* 294:571–574.
15. Zhang B, et al. (2017) Observation of giant conductance fluctuations in a protein. *Nano Futures* 1:035002.
16. Tuchband M, He J, Huang S, Lindsay S (2012) Insulated gold scanning tunneling microscopy probes for recognition tunneling in an aqueous environment. *Rev Sci Instrum* 83:015102.
17. Chang S, He J, Zhang P, Gyarfas B, Lindsay S (2011) Gap distance and interactions in a molecular tunnel junction. *J Am Chem Soc* 133:14267–14269.
18. Chang S, et al. (2012) Chemical recognition and binding kinetics in a functionalized tunnel junction. *Nanotechnology* 23:235101.
19. Smith T (1980) The hydrophilic nature of a clean gold surface. *J Colloid Interface Sci* 75:51–55.
20. Leary E, et al. (2011) Unambiguous one-molecule conductance measurements under ambient conditions. *Nano Lett* 11:2236–2241.
21. Ruiz MP, et al. (2017) Bioengineering a single-protein junction. *J Am Chem Soc* 139:15337–15346.
22. Weber PC, Ohlendorf DH, Wendoloski JJ, Salemme FR (1989) Structural origins of high-affinity biotin binding to streptavidin. *Science* 243:85–88.
23. Sano T, Cantor CR (1990) Cooperative biotin binding by streptavidin. Electrophoretic behavior and subunit association of streptavidin in the presence of 6 M urea. *J Biol Chem* 265:3369–3373.
24. Xiao X, Xu B, Tao N (2004) Conductance titration of single-peptide molecules. *J Am Chem Soc* 126:5370–5371.
25. Giese B, Spichty M (2000) Long distance charge transport through DNA: Quantification and extension of the hopping model. *ChemPhysChem* 1:195–198.
26. Giese B, Amaudrut J, Köhler AK, Spormann M, Wessely S (2001) Direct observation of hole transfer through DNA by hopping between adenine bases and by tunnelling. *Nature* 412:318–320.
27. Harriman A (1987) Further comments on the redox potentials of tryptophan and tyrosine. *J Phys Chem* 91:6102–6104.
28. Odella E, et al. (2018) Controlling proton-coupled electron transfer in bioinspired artificial photosynthetic relays. *J Am Chem Soc* 140:15450–15460.
29. Tripkovic V, Björketun ME, Skúlason E, Rossmeisl J (2011) Standard hydrogen electrode and potential of zero charge in density functional calculations. *Phys Rev B Condens Matter Mater Phys* 84:115452.
30. Alloway DM, et al. (2003) Interface dipoles arising from self-assembled monolayers on gold: UV-photoemission studies of alkanethiols and partially fluorinated alkanethiols. *J Phys Chem B* 107:11690–11699.
31. Guo C, et al. (2016) Tuning electronic transport via hepta-alanine peptides junction by tryptophan doping. *Proc Natl Acad Sci USA* 113:10785–10790.
32. Vattay G, Salahub D, Csabai I, Nassimi A, Kaufmann SA (2015) Quantum criticality at the origin of life. *J Phys Conf Ser* 626:012023.
33. Lagunas A, et al. (2018) Long distance electron transfer through the aqueous solution between redox partner proteins. *Nat Commun* 9:5157.
34. Jeffrey GA (1997) *An Introduction to Hydrogen Bonding* (Oxford Univ Press, New York).
35. Choi Y, et al. (2012) Single-molecule lysozyme dynamics monitored by an electronic circuit. *Science* 335:319–324.